AGU PUBLICATIONS

Geochemistry, Geophysics, Geosystems

RESEARCH ARTICLE
10.1002/2016GC006576

Metamorphic records for subduction erosion and subsequent underplating processes revealed by garnet-staurolite-muscovite schists in central Qiangtang, Tibet

Xiu-Zheng Zhang[1], Yong-Sheng Dong[2], Qiang Wang[1,3], Wei Dan[1,3], Chunfu Zhang[4], Wang Xu[2], and Ming-Liang Huang[5]

[1]State Key Laboratory of Isotope Geochemistry, Guangzhou Institute of Geochemistry, Chinese Academy of Sciences, Guangzhou, China, [2]College of Earth Science, Jilin University, Changchun, China, [3]CAS Center for Excellence in Tibetan Plateau Earth Science, China, [4]Department of Geosciences, Fort Hays State University, Hays, Kanas, USA, [5]State key Laboratory of Ore Deposit Geochemistry, Institute of Geochemistry, Chinese Academy of Sciences, Guiyang, China

Abstract Subduction erosion is confirmed as a crucial geodynamic process of crustal recycling based on geological, geochemical, and geophysical observations at modern convergent plate margins. So far, not a single metamorphic record has been used for constraining a general tectonic evolution for subduction erosion. Here we first revealed metamorphic records for a subduction erosion process based on our study of the Late Paleozoic garnet-staurolite-muscovite schists in the central Qiangtang block, Tibet. Provenance analyses suggest that the protoliths of garnet-staurolite-muscovite schists have the Northern Qiangtang-affinity and were deposited in an active continental margin setting. Mineral inclusion data show that the early metamorphic stage (M_1) recorded blueschist facies pressure-temperature (P-T) conditions of 0.8–1.1 GPa and 402–441°C, indicating that a part of the material from the overriding plate had been abraded into the subduction channel and undergone high-pressure/low-temperature metamorphism. The peak metamorphic stage (M_2) recorded amphibolite facies P-T conditions of 0.3–0.5 GPa and 470–520°C. The $^{40}Ar/^{39}Ar$ cooling ages (263–259 Ma) yielded from muscovite suggest the amphibolite facies metamorphism (>263 Ma) occurred at oceanic subduction stage. The distinctly staged metamorphism defines a clockwise and warming decompression P-T-t path which reveals an underplating process following the early subduction erosion. During the tectonic process, the eroded low-density material escaped from the cold subduction channel and rise upward into the warm middle-lower crust of the upper plate, undergoing amphibolite facies metamorphism. Our new results revealed a complete evolutional process from the early subduction erosion to the subsequent underplating during the northward subduction of the Paleo-Tethys Ocean.

Key Points:
- Distinct P-T-t path revealed a complete processes from subduction erosion to subsequent underplating
- Robust evidence of subduction erosion during the northward subduction of the Paleo-Tethys Ocean
- Metamorphic indicator for determining a subduction erosion process in the other fossil subduction zones

Supporting Information:
- Supporting Information S1

Correspondence to:
X.-Z. Zhang,
zhangxz@gig.ac.cn;
Q. Wang,
wqiang@gig.ac.cn

Citation:
Zhang, X.-Z., Y.-S. Dong, Q. Wang, W. Dan, C. Zhang, W. Xu, and M.-L. Huang (2017), Metamorphic records for subduction erosion and subsequent underplating processes revealed by garnet-staurolite-muscovite schists in central Qiangtang, Tibet, *Geochem. Geophys. Geosyst.*, *18*, 266–279, doi:10.1002/2016GC006576.

Received 4 AUG 2016
Accepted 22 DEC 2016
Accepted article online 3 JAN 2017
Published online 25 JAN 2017

1. Introduction

Subduction erosion, by frontal and basal removal of crustal material from the overriding plate, is widely accepted as a fundamental process of crustal recycling at nearly all current convergent plate margins [*von Huene and Scholl*, 1991; *Ranero and von Huene*, 2000; *von Huene et al*., 2004; *Scholl and von Huene*, 2009]. Globally, it accounts for nearly one-third of the ~5.25 km^3 of continental crust recycled back into the mantle annually among a series of crustal consumption processes (e.g., continental delamination, continental collision, and loss of chemical solute) [*Clift et al*., 2009; *Stern*, 2011]. Previous researches focused on the identification of subduction erosion in active continental margins, the mechanisms causing the subduction erosion, and the implications for supercontinent cycle and arc magmas [*von Huene and Scholl*, 1991; *Ranero and von Huene*, 2000; *von Huene et al*., 2004; *Goss and Kay*, 2006; *Vannucchi et al*., 2013; *Tonarini et al*., 2011; *Scholl and von Huene*, 2009; *Clift et al*., 2009; *Stern*, 2011; *Holm et al*., 2014; *Zhang et al*., 2012; *Liu et al*., 2014]. However, the general tectonic evolution and recycling process of materials abraded by subduction erosion remain enigmatic. This is partially due to a lack of crucial metamorphic records (P-T-t paths) which can reveal a complete tectonic evolutionary history for a general subduction erosion process.

The Qiangtang block in central Tibet exposes a >500 km long, east-west trending tectonic mélange belt (QTMB) (Figure 1), which recorded the long-time subduction and final closure history of Paleo-Tethys Ocean [*Kapp et al*., 2000; *Zhang et al*., 2006a, 2006b, 2014b, 2014c, 2016; *Zhai et al*., 2011a, 2011b, 2013a, 2016;

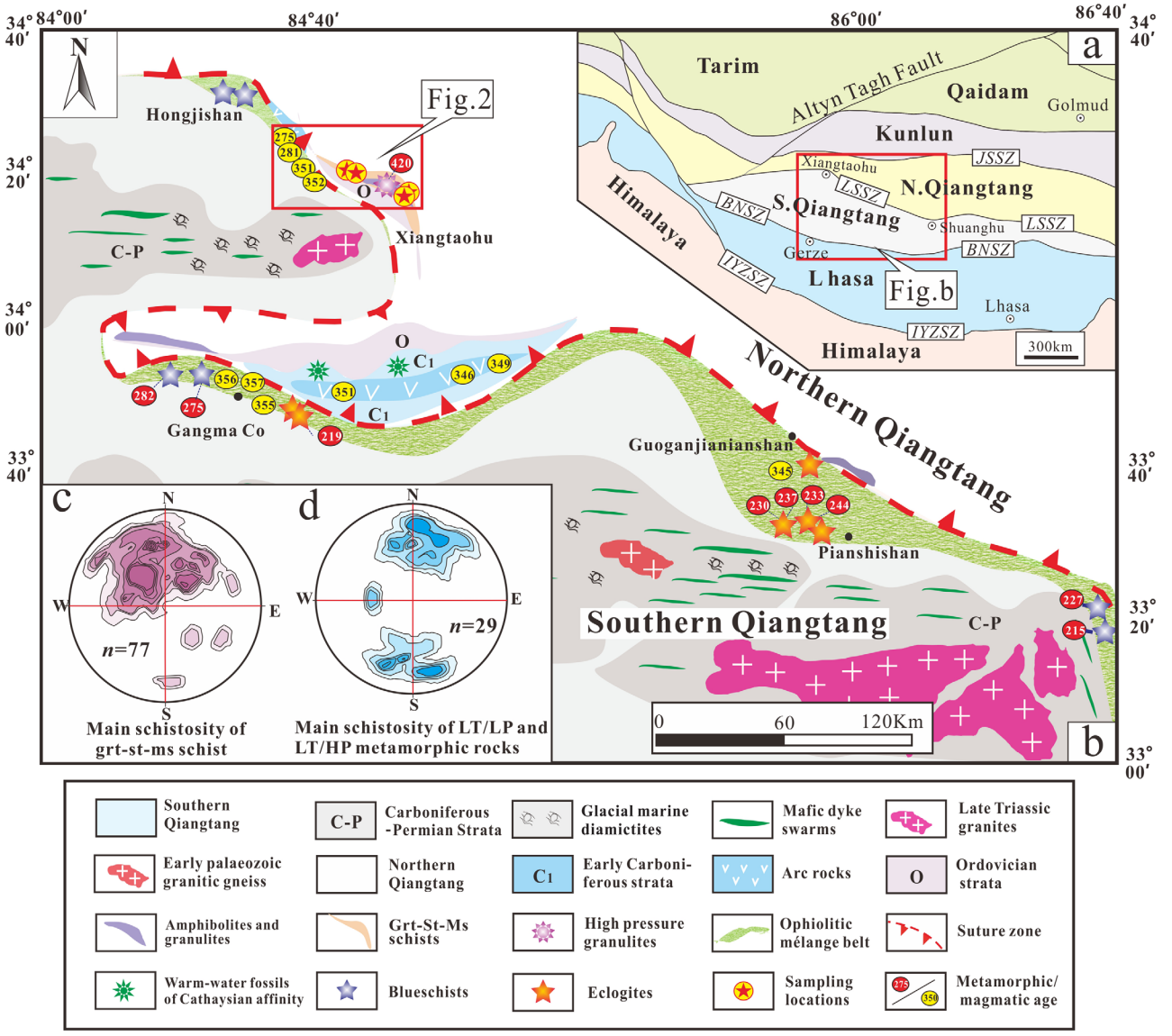

Figure 1. (a) Sketch map of Tibet (modified after *Zhai et al.* [2011a]), showing the distribution of the main suture zones. (b) Simplified geological map of the Qiangtang area, central Tibet (adapted from *Zhang et al.* [2014a, 2016]). (c and d) Stereographic plots (equal-area, lower hemisphere projection) showing the schistosity orientations of the Grt-St-Ms schists (c) and the LT/HP (LP) metamorphic rocks (d) from the central Qiangtang Block. JSSZ = Jinsha Suture Zone; LSSZ = Longmu Co-Shuanghu Suture Zone; BNSZ = Bangong-Nujiang Suture Zone; IYZSZ = Indus-Yarlung Zangbo Suture Zone. The metamorphic and magmatic ages are from: *Zhai et al.* [2011a, 2013a], *Deng et al.* [2000], *Pullen et al.* [2008], *Tang and Zhang* [2014], *Jiang et al.* [2014], and *Zhang et al.* [2014a, 2016].

Jiang et al., 2015; *Metcalfe*, 2013]. It seems to be an ideal natural laboratory for investigating crustal recycling associated with the subduction factory. The QTMB is dominated by low-temperature/high-pressure (LT/HP) (e.g., eclogites and blueschists) and low-temperature/low-pressure (LT/LP) (greenschist facies) metamorphic rocks [*Li and Zheng*, 1993; *Li et al.*, 2006; *Kapp et al.*, 2000, 2003; *Pullen et al.*, 2008; *Zhang et al.*, 2006a, 2006b; *Tang and Zhang*, 2014; *Zhai et al.*, 2011a]. Here we report a set of amphibolite facies metamorphic rocks (garnet-staurolite-muscovite schists) related to the evolution of Paleo-Tethys Ocean from the Xiangtao Lake area, in central Qiangtang, Northern Tibet. This paper is to give a detailed account of the petrological features, mineralogical data, detrital zircon ages, and $^{40}Ar/^{39}Ar$ dating for these metamorphic rocks. The results were used to constrain a distinct metamorphic record which revealed a complete evolutional history of a process from the early subduction erosion to the subsequent underplating process during the northward subduction of the Paleo-Tethys Ocean.

2. Geological Setting and Field Occurrence

Tibet is composed of several continental blocks (Figure 1) that progressively accreted to Asia as a result of the closure of the intervening Tethyan oceans (Paleo-Tethys to Ceno-Tethys) throughout the Paleozoic to Mesozoic Eras [*Yin and Harrison*, 2000; *Metcalfe*, 2013; *Zhu et al*., 2013]. The Qiangtang block is situated in the central part of the Tibetan Plateau, which is bounded by the Bangong-Nujiang suture zone to the south and the Jinsha suture zone to the north (Figures 1a and 1b) [*Yin and Harrison*, 2000]. The Qiangtang block is subdivided into the Northern and Southern Qiangtang blocks (NQB and SQB) with different affinities by Longmu Co-Shuanghu Suture zone (LSSZ) [Li, 1987; *Li and Zheng*, 1993; *Metcalfe*, 2013]. To the north side of the LSSZ, the NQB consists mainly of Late Devonian to Triassic sedimentary sequences, most of which have been overlain by Jurassic to Cenozoic sedimentary rocks [*Li*, 1987; *Li and Zheng*, 1993]. Some Late Paleozoic sedimentary rocks contain abundant warm-water fossils of a Cathaysian affinity [*Li and Zheng*, 1993; *Zhang et al*., 2009; *Peng et al*., 2014]. In contrast, the SQB is characterized by Carboniferous to Permian glaciomarine deposits with cold-water biota, which are typical indicators of a Gondwanan affinity [*Li and Zheng*, 1993; *Metcalfe*, 2013; *Fan et al*., 2015]. The LSSZ, first proposed by *Li* [1987] as an in situ Triassic suture zone (Figures 1a and 1b), is composed of blueschists, eclogites, ophiolites, OIB-type basalts, metasedimentary rocks, and minor chert [*Kapp et al*., 2000, 2003; *Li et al*., 2006; *Zhang et al*., 2006a, 2006b; *Zhai et al*., 2011a, 2013a, 2016; *Zhang et al*., 2014b, 2016], and it continues to be regarded as the relic of the main Paleo-Tethys Ocean [*Zhai et al*., 2011a, 2011b, 2013a; *Metcalfe*, 2013; *Zhu et al*., 2013; *Zhang et al*., 2016]. The timing of closure of the Paleo-Tethys Ocean and continental collision has been constrained as Middle to Late Triassic based on paleolatitude [*Song et al*., 2015], ages of LT/HP rocks [*Zhai et al*., 2011a; *Pullen et al*., 2008], and postcollision magma [*Zhang et al*., 2014c].

The Xiangtao Lake area, located in the western segment of the LSSZ (Figures 1b and 2), is a complex consisting of Carboniferous-Permian ophiolites, blueschists, Ordovician metasedimentary rocks, and Early Paleozoic basic amphibolites-high-pressure granulites (middle-lower crust of Northern Qiangtang) [*Zhang et al*., 2014a, 2016] overlain by Triassic to Cenozoic unmetamorphosed sedimentary rocks (Figures 2a and 2b). The garnet-staurolite-muscovite (Grt-St-Ms) schists newly discovered in the Xiangtao Lake area are distributed in a 8–10 km long by ~1 km wide, NE-SW trending belt, and is in fault contact with the Ordovician metasedimentary rocks to the northwest, and with Early Paleozoic high-pressure granulites and amphibolites to the southeast [*Zhang et al*., 2014a, 2016] (Figures 2a and 2b). The Grt-St-Ms schists are characterized by the occurrence of amphibolite facies diagnostic minerals (e.g., staurolite) with NE-SW trending penetrative schistosity (S_2). These features (Figure 1c) are inconsistent with the vast majority of rocks in the QTMB which have generally experienced LT/HP and LT/LP metamorphism with the main W-E trending schistosity (Figure 1d).

3. Sample Description and Petrography

The Grt-St-Ms schists investigated here are mainly composed of muscovite (Ms) (30–35 vol %), quartz (Qtz) (25–30 vol %), garnet (Grt) (10–15 vol %), staurolite (St) (10–15 vol %), biotite (Bt) (~7 vol %), plagioclase (Pl) (~5 vol %), phengite (Phen) (<5 vol %), K-feldspar (Kfs) (<5 vol %), and minor accessory mineral (e.g., monazite, zircon) (Figures 3a–3d). In samples L1217 and TL21, minor fine-grained phengite ($Phen_I$) and oriented quartz (Qtz_I) occurs as small inclusions in the mantle of garnet porphyroblasts which define the early schistosity (S_1) (Figure 3b). Inclusion trails (S_1) are oriented at a high angle to the matrix schistosity (S_2) that is defined by muscovite, staurolite porphyroblast, quartz, and biotite in the matrix. In samples L1205 and L1218, the relic early schistosity (S_1) are defined by minor relic phengite in the matrix which are also oriented at a high angle to the main schistosity (S_2) (Figure 3d).

4. Results

Analytical methods are described in the supporting information Text S1. The representative mineral compositions, zircon U-Pb data, $^{40}Ar/^{39}Ar$ dating data, and the calculation results of P-T conditions for the Grt-St-Ms schists are listed in the supporting information Tables S1–S4, respectively.

4.1. Mineral Compositions

4.1.1. Garnet

Garnet porphyroblasts from the Grt-St-Ms schists are euhedral to subhedral and have been rotated by shearing along the main schistosity (S_2) (Figure 3c), suggesting that they were mainly formed in the early

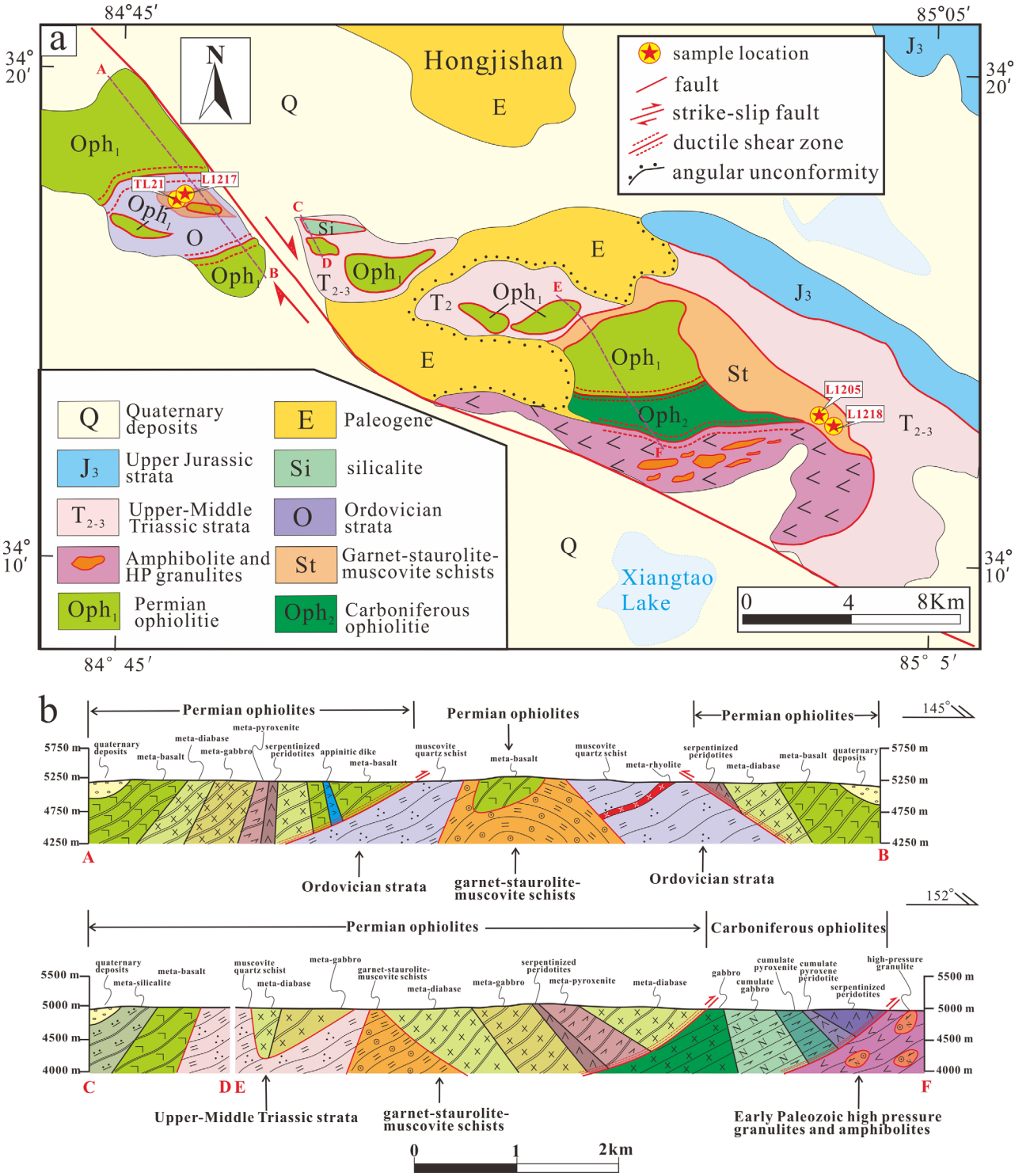

Figure 2. (a) Geologic maps of the Xiangtao Lake areas, showing outcrops of the garnet-staurolite-muscovite schists and the sample locations for zircon U-Pb and $^{40}Ar/^{39}Ar$ dating (modified from *Zhang et al.* [2014a]). The dashed lines (AB, CD, and EF) are cross sections; (b) structural cross-sections for Xiangtaohu area from central Qiangtang, Tibet (modified from *Zhang et al.* [2016]).

metamorphic stage. They are characterized by high FeO, low MgO, and varying CaO and MnO contents (supporting information Table S1), and show irregular compositional zoning ($Alm_{79–83}Prp_{9–11}Grs_{4–12}Sps_{0.1–4}$). Compositional map of a garnet porphyroblast from a representative sample (TL21) reveal a decrease spessartine from core (3–4 mol %) to rim (0.1–0.6 mol %), and nearly homogeneous pyrope (9–11 mol %) and

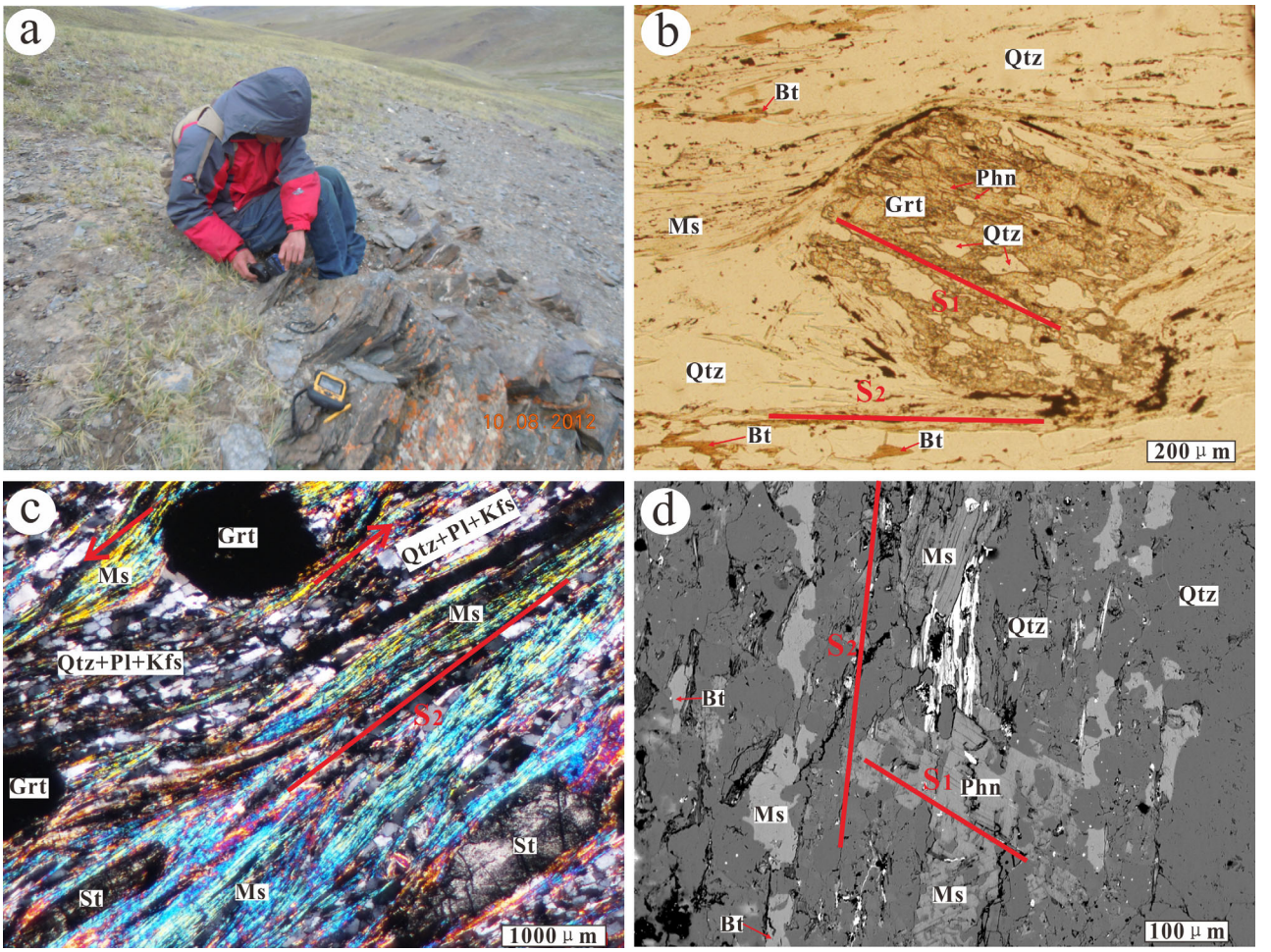

Figure 3. (a) Field photographs showing the occurrences of the Grt-St-Ms schists from the Xiangtao Lake area. (b) In the early blueschist facies, the index mineral assemblage (M_1) of phengite ($Phen_I$) and oriented quartz (Qtz_I) occur as small inclusions in garnet porphyroblasts and define the early schistosity (S_1). S_1 Inclusion trails are oriented at a high angle to the matrix schistosity (S_2) (plane polarized light photomicrograph). (c) The peak mineral assemblage of muscovite + staurolite + biotite + quartz + plagioclase ± potassium feldspar identified in the matrix of the Grt-St-Ms schists which define the main schistosity (S_2) (crossed polarized light photomicrograph). (d) The relic early schistosity (S_1) is defined by minor relic phengite in the matrix which are also oriented at a high angle to the main schistosity (S_2) (back-scattered electron images).

almandine content (79–83 mol %) (Figure 4a). Furthermore, the garnets have varying grossular contents (4–12 mol %) and their mantle close to the inclusions ($Phen_I + Qtz_I$) generally have the highest Ca contents (X_{grs} = 10–12).

4.1.2. White Micas

The white micas from the Grt-St-Ms schists include phengites and muscovites. The phengites occur as small inclusions in garnet porphyroblasts or minor relic minerals in the matrix, and they formed the early schistosity (S_1). They are characterized by low Al_2O_3 (26.14–29.13 wt %) and high Si values (3.45–3.56 p.f.u. [per formula units]) (supporting information Table S1). Their compositions are similar to those in the LT/HP rocks resulted from oceanic subduction from the QTMB (e.g., eclogites, blueschists, and garnet-phengite schists) (Figure 4b). In contrast, the white micas in the matrix are dominated by muscovite in intergrowths with staurolite and biotite, suggesting a mineral assemblage of medium temperature and pressure condition. Meanwhile, they have relatively high Al_2O_3 (35.56–36.72 wt %) and lower Si values (3.12–3.17 p.f.u.), which are similar to those in rocks formed in amphibolite facies (Figure 4b).

4.1.3. Staurolite

Staurolite porphyroblasts are euhedral to subhedral prismatic in shape, which defines an axial planar matrix schistosity (S_2). They have varying SiO_2 (25.92–28.83 wt %), and R^{2+} (Mg + Fe + Zn + Mn + Co + Ni) contents (Figure 4c), and $A1_2O_3$ (49.76–57.42 wt %), TiO_2 (0.25–0.50 wt %), and X_{Mg} (0.12–0.16). The cores of staurolites are characterized by the relatively high Al (17.67–18.26 p.f.u.) and low Si values (7.41–7.71 p.f.u.),

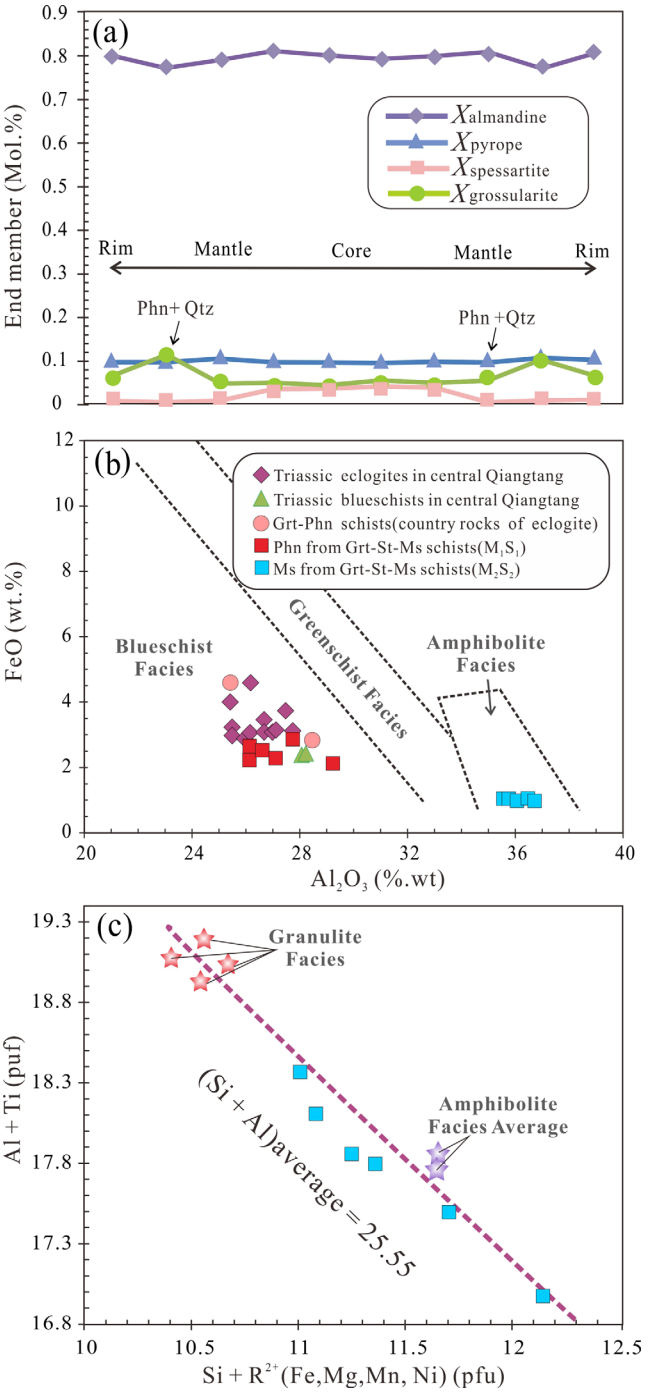

Figure 4. (a) Core-rim compositional profile for the garnet porphyroblasts from the Grt-St-Ms schists. (b) Relationship between FeO and Al_2O_3 of white mica, showing variations of white mica formed under different metamorphic conditions. (c) Plot of Al + Ti versus Si + R^{2+} (Fe, Mg, Zn, Mn, Co, Ni) of staurolites. The data of granulite-facies and amphibolite-facies staurolites are from *Hiroi et al.* [1994].

which are consistent with the characteristics of ordinary amphibolite facies staurolites [*Hiroi et al.* 1994]. By comparison, the rims of staurolites have relatively low Al (16.68–17.74 p.f.u.) and high Si values (7.89–8.30 p.f.u.) which may be modified by retrograde metamorphism during late cooling stage.

4.1.4. Other Minerals

Biotite occurs in the matrix as fine-grained scales, and is characterized by X_{Mg} values ranging from 0.31 to 0.36 and TiO_2 contents varying from 1.22 to 1.44 wt %. Plagioclase and K-feldspar occur as fine-grained crystals in the quartz-rich layers of the matrix. Plagioclase's composition is $An_{46–48}Ab_{50–51}Or_{2–3}$, and K-feldspar has a composition of $An_0Ab_{4–8}Or_{96–98}$.

4.2. Detrital Zircon Age Distribution

Most zircon grains from Grt-St-Ms schist samples (TL21 and L1205) are of magmatic origin, exhibiting variable grain sizes of ~80 to 200 μm and clear oscillatory zoning in cathodoluminescence (CL) images (Figures 5b and 5d). Some magmatic zircons are surrounded by metamorphic rims (2–5 μm) with moderate-luminescence to high-luminescence (Figure 5d) but the rims are too narrow to be analyzed. All the detrital zircon age data yield from magmatic zircon grains are presented in supporting information Table S2 and exhibited in Figure 5. The $^{207}Pb/^{206}Pb$ ages were used for those older than 1000 Ma, and $^{206}Pb/^{238}U$ ages were used for younger zircons. Meanwhile, all the results cited in this study exclude analyses with >10% discordance [*Gehrels et al.*, 2011]. The sample L1205 yielded ages ranging from 346 to 2389 Ma which have a main peak at ca. 360 Ma and a subpeak at 452 Ma (Figures 5a and 5b). The sample TL21 have the similar detrital zircon spectra (2272–349 Ma), main peak (ca. 357 Ma), and subpeak (ca. 422 Ma) (Figures 5c and 5d). These age distribution patterns are almost exactly the same as those from the Early Carboniferous strata in the Northern Qiangtang Block [*Peng et al.*, 2014].

4.3. $^{40}Ar/^{39}Ar$ Dating Results

The results of $^{40}Ar/^{39}Ar$ dating are shown in supporting information Table S3. The muscovite samples from Grt-St-Ms schists yielded well-defined plateau ages of 258.9 ± 1.6 Ma (L1217) and 263.3 ± 1.8 Ma (L1218)

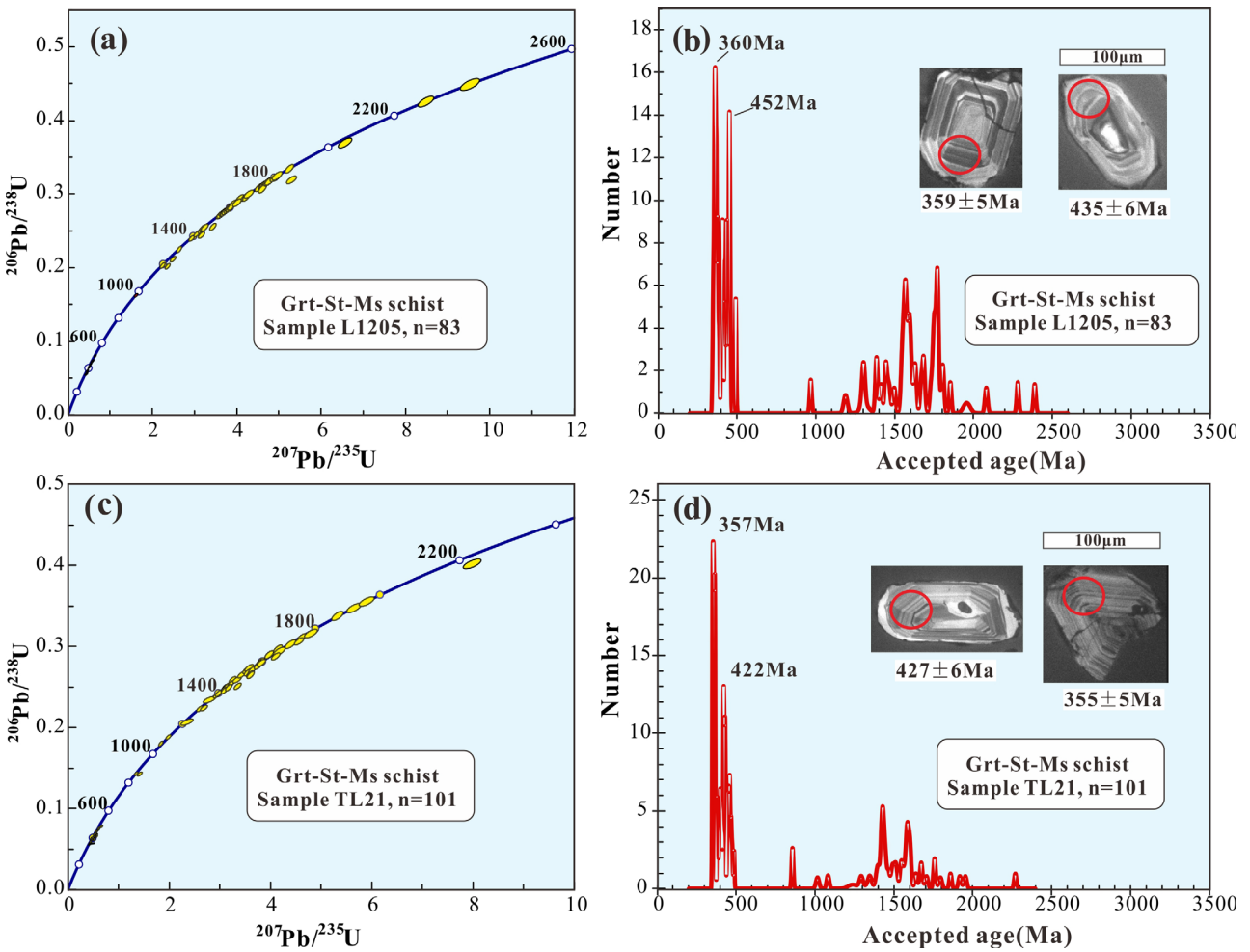

Figure 5. Zircon U-Pb concordia diagrams and cathodoluminescence (CL) images for Grt-St-Ms schists (L1205 and TL21) from the central Qiangtang Block, central Tibet.

(Figure 6). The initial $^{40}Ar/^{36}Ar$ values for these two samples (L1217 and L1218) are consistent with the atmospheric value (295.5) within analytical error (supporting information Figure S1). This and the agreement between the plateau and isochron ages (Figure 6 and supporting information Figure S1) indicate the absence of an excess argon component in the muscovite.

5. Discussion

5.1. Thermobarometric Evaluation

Based on inclusions, mineral textures, and mineral chemistry, two metamorphic stages for Grt-St-Ms schists have been recognized: the early LT/HP metamorphic assemblage (M_1), and the peak amphibolite facies assemblage (M_2).

The early metamorphic stage (M_1) is represented by inclusion assemblages of fine-grained phengite and oriented quartz within the Ca-rich mantle of garnet porphyroblasts (Figures 3b and 3d). The P-T conditions are calculated from thermometers for garnet + phengite [*Krogh and Råheim*, 1978] and phengite geobarometry [*Velde et al.*, 1967; *Massonne and Schreyer*, 1987], utilizing the compositions of phengite and the adjacent Ca-rich garnet mantle. The Grt-St-Ms schist samples yielded a P-T range of 0.8–1.1 GPa and 402–441°C (supporting information Table S4), which is representative of the metamorphic conditions during the blueschist facies prograde metamorphism stage (M_1).

The characteristic peak mineral assemblage is staurolite + muscovite + garnet (rim) + biotite + quartz + plagioclase ± potassium feldspar. The P-T conditions have been calculated using thermometers for

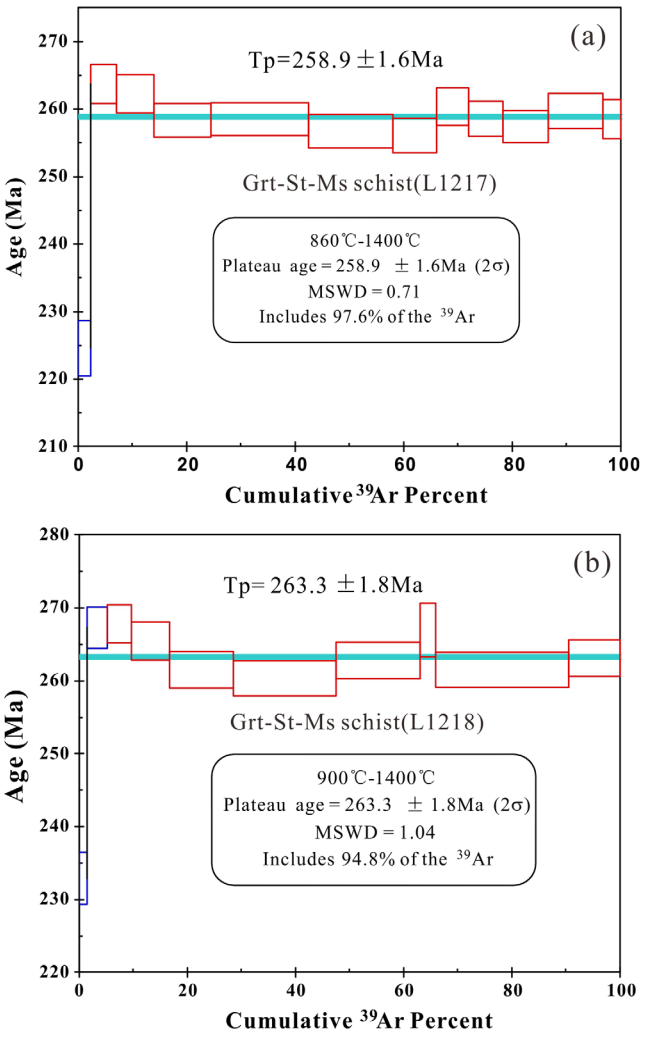

Figure 6. $^{40}Ar/^{39}Ar$ plateau and isochronal ages for the muscovite samples from the Grt-St-Ms schists (L1217 and L1218).

garnet + muscovite [*Krogh et al.*, 1978], Ti-in-muscovite thermometers [*Wu and Chen*, 2015], and geobarometers for the garnet + muscovite + plagioclase + quartz assemblage [*Wu and Zhao*, 2006]. The samples investigated in this study yielded a P-T range of 0.3–0.5 GPa and 470–520°C (supporting information Table S4), representing the peak P-T conditions of the amphibolite facies stage (M_2).

5.2. Provenance Analysis: Fossil Active Continental Margin

Compilations of crystallization ages for detrital zircons from the Grt-St-Ms schist samples (TL21 and L1205) and the Early Carboniferous strata (Riwanchaka formation, C_1r) of the Northern Qiangtang Block [*Peng et al.*, 2014] show extremely similar patterns of peaks (~360 Ma) and troughs, although with slight variations in the relative amplitudes of the subpeaks (Figure 7). This similarity of detrital zircon age patterns suggests that the zircons have a similar clastic source. It is noteworthy that a large proportion of detrital zircons with ages of ca. 360 Ma from both the Grt-St-Ms schists and the Early Carboniferous strata of the Northern Qiangtang Block [*Peng et al.*, 2014] are euhedral to subhedral in shape and exhibit good oscillatory zoning, which is a typical feature of magmatic zircons from intermediate-acidic magmas (Figure 5) [*Hoskin and Black*, 2000]. Based on the available data, the early Carboniferous magmas are only distributed in the Northern Qiangtang Block (arc volcanic lava, ~350 Ma), which is regarded as the result of northward subduction of the Paleo-Tethys Ocean [*Jiang et al.*, 2015]. So far, the Early Carboniferous magmas and even the individual detrital zircon grains with Carboniferous ages are absent from the Southern Qiangtang Block (Figure 7). Hence, the protoliths of the Grt-St-Ms schists should have the Northern Qiangtang-affinity.

Detrital zircon spectra are also regarded as indicators of tectonic settings of the basin in which the zircons are deposited [*Cawood et al.*, 2012]. Generally, samples from the Early Carboniferous strata of the Northern Qiangtang Block [*Peng et al.*, 2014] are characterized by a majority of zircon ages approaching the time of sediment accumulation (measured crystallization age [CA]—depositional age [DA] < 100 Ma at 30% of the zircon population, Figure 8), which is consistent with an active continental margin setting (Figure 8) [*Cawood et al.*, 2012]. Synsedimentary arc magmatic activity [*Jiang et al.*, 2015] is likely the source of the youngest detrital zircon grains. In contrast, samples from the Carboniferous-Permian strata of the Southern Qiangtang Block [*Fan et al.*, 2015; *Gehrels et al.*, 2011] contain more zircons with older ages (CA–DA > 150 Ma at 5% of the zircon population, Figure 8) that mainly derived from the underlying basement and is indicative of a passive continental margin setting [*Cawood et al.*, 2012]. The Grt-St-Ms schist samples with unknown origins (TL21 and L1205) in this study contain a large proportion of zircon grains (>30%) with ages within 100 Ma ($CA–DA_{max}$) and 150 Ma ($CA–DA_{min}$) of the host sediment, if the youngest detrital zircon grains (mean = ~350 Ma, $n = 3$) and $^{40}Ar/^{39}Ar$ cooling ages (ca. 261 Ma) were used as maximum and

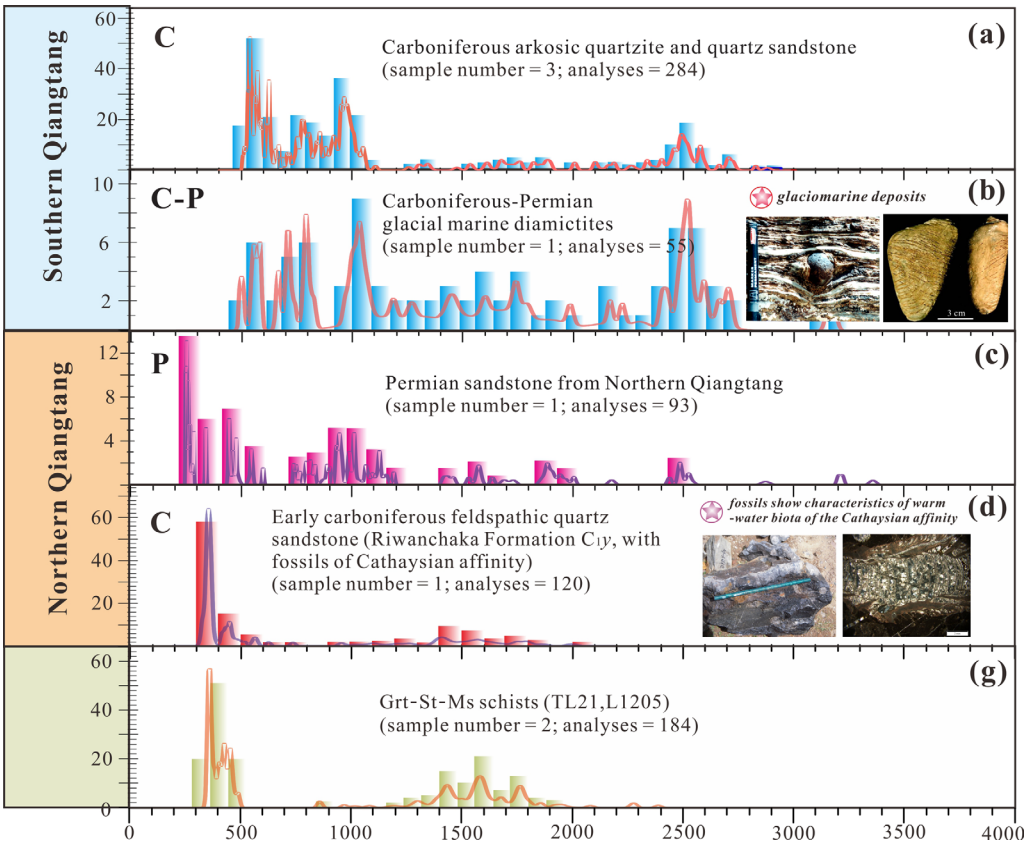

Figure 7. Summary of detrital zircon age distributions from standard strata of the (a and b) Southern and (c and d) Northern Qiangtang Blocks [*Gehrels et al.*, 2011; *Fan et al.*, 2014; *Peng et al.*, 2014] and (e) metamorphic rocks (this study).

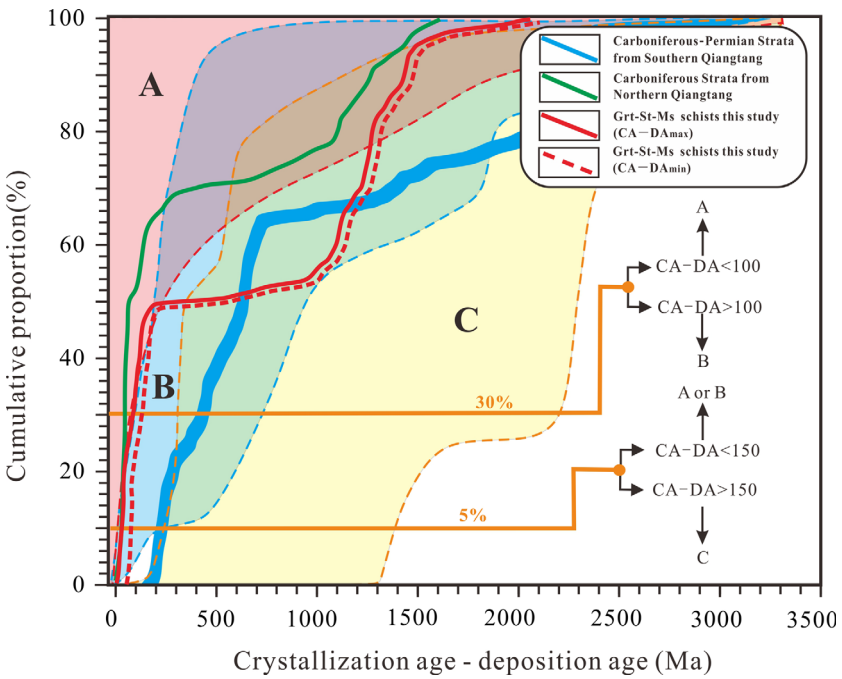

Figure 8. Discrimination diagrams of detrital zircon age patterns for determining their tectonic settings (modified from *Cawood et al.* [2012]). (a) convergent (red field); (b) collisional (blue field); (c) extensional (yellow field).

minimum depositional ages (DA_{max} and DA_{min}), respectively (supporting information Table S4 and Figure 8). These features are consistent with an active continental margin and/or collisional setting, but apparently opposite to a passive margin setting [*Cawood et al.*, 2012]. Considering that the Paleo-Tethys Ocean closed and continental collision occurred during the Late Triassic [*Song et al.*, 2015; *Zhai et al.*, 2011a; *Pullen et al.*, 2008; *Zhang et al.*, 2014c], the late Permian collisional setting can be ruled out.

In summary, the Grt-St-Ms schist samples (TL21 and L1205) have remarkably similar detrital zircon spectra to those from the Carboniferous strata of the Northern Qiangtang Block, and contain a large proportion of zircons with ages close to the time of sediment and synsedimentary arc magmatic activity [*Jiang et al.*, 2015]. These features suggest that the protoliths of the Grt-St-Ms schists have the Northern Qiangtang-affinity and were deposited in an active continental margin setting.

5.3. Metamorphic Records (P-T-t Path) of Subduction-Erosion

The petrographic textures, mineral compositions, thermobarometry, and $^{40}Ar/^{39}Ar$ data of the Grt-St-Ms schists define a clockwise P-T-t path, including a distinct warming decompression stage which is significantly different from those of LT/HP metamorphic rocks (eclogites and blueschists; summarized in Figure 9a) in the central Qiangtang Block [*Zhai et al.*, 2011a; *Tang and Zhang*, 2014]. The early blueschist facies were determined to have P-T conditions of 0.8–1.1 GPa and 402–441°C (low gradient of ~10°C/km), which were estimated from the phengite (inclusion) + quartz (inclusion) + Ca-rich garnet assemblage (M_1), suggesting a typical subduction zone setting [e.g., *Ernst*, 1988; *Stern*, 2005]. Moreover, the protoliths of the Grt-St-Ms schists have the Northern Qiangtang-affinity and the Northern Qiangtang block continues to be regarded as an active continental margin setting based on occurrence of the arc magmatic activities [*Yang et al.*, 2011; *Zhai et al.*, 2013b; *Jiang et al.*, 2015]. These new results suggest that a part of the crustal material from the overriding plate had been abraded into the subduction channel, subducted to a depth of ~40 km, and undergone LT/HP metamorphism (Figure 9b). This provides robust evidence of subduction erosion during the northward subduction of the Paleo-Tethys Ocean.

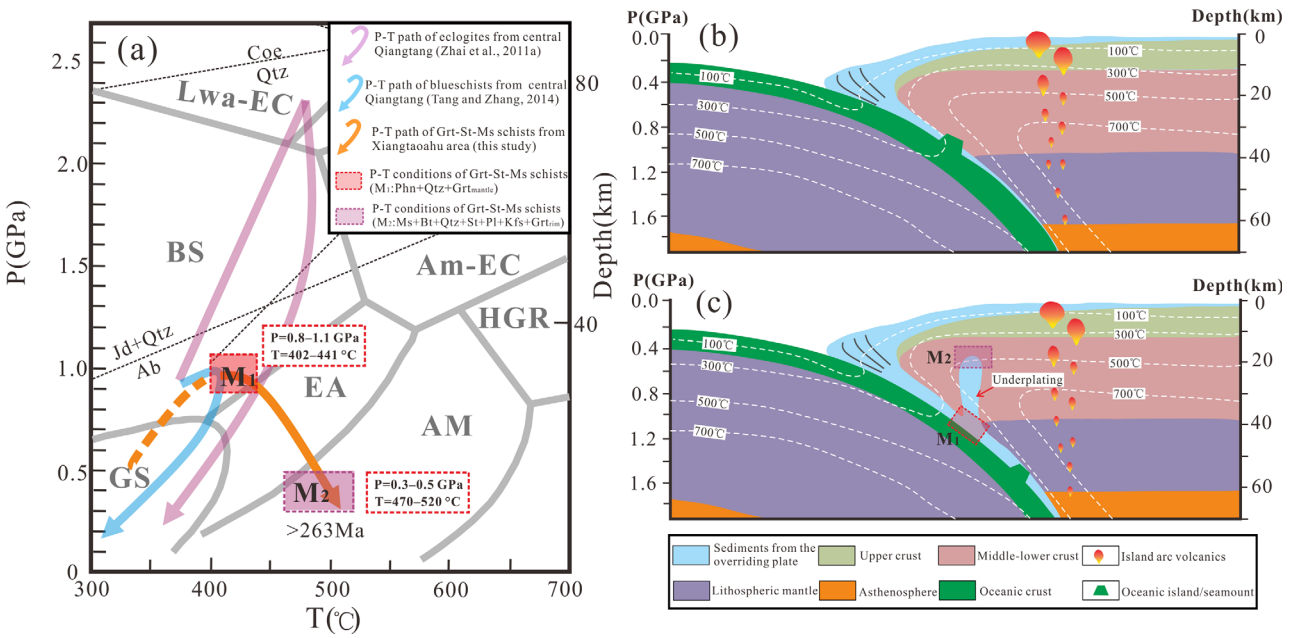

Figure 9. (a) P-T-t path for Grt-St-Ms schists (orange arrow) from the central Qiangtang Block, central Tibet. The geotherms and the metamorphic facies fields are after *Zhai et al.* [2011a]. The Grt-St-Ms schists are distinguished by a clockwise and warming decompression P-T-t path which is significantly different from those of eclogites (purple arrow, *Zhai et al.* [2011a]) and blueschist (blue arrow, *Tang and Zhang* [2014]). (b) Cartoon illuminating the subduction erosion in response to the subduction of seamounts (or oceanic islands) during the ongoing northward subduction of the Paleo-Tethys Ocean. (c) The distinct metamorphic evolution (P-T-t path) of Grt-St-Ms schists reveals an underplating process by which the low-density materials escaped from the cold subduction channel (~10°C/km) and intruded into the hot middle-lower crust of the overriding plate (>25°C/km) and underwent amphibolite facies metamorphism. The geothermal gradients (white line) of the subduction channel and the overriding plate are estimated from the LT/HP metamorphic rocks [*Kapp et al.*, 2000; *Li et al.*, 2006; *Zhang et al.*, 2006; *Zhai et al.*, 2011a; *Tang and Zhang*, 2014] and the Early Paleozoic basic amphibolites-high-pressure granulites (middle-lower crust of Northern Qiangtang) [*Zhang et al.*, 2014a], respectively.

Subduction erosion has been accepted as a fundamental process which thins and reduces the volume of the wedge above the subducted plate through the frontal erosion and/or basal erosion processes [*von Huene and Scholl*, 1991; *Ranero and von Huene*, 2000; *von Huene et al*., 2004; *Stern*, 2011]. Its mechanisms mainly include: (1) hydrofracturing of the upper plate's framework rocks due to fluid overpressure (detached from the subducted oceanic crust) in and above the subduction channel [e.g., *Stern*, 2011]; (2) large subduction zone earthquakes [e.g., *Wang et al*., 2010]; and (3) subduction of buoyant features such as oceanic ridges, seamounts, and oceanic island arcs [e.g., *Kukowski and Oncken*, 2006; *Stern*, 2011]. In particular, subduction of buoyant features can result in rapid pulses of subduction erosion by the disaggregation of the framework rocks of the upper plate, enhancing hydrofracturing, and widening the subduction channel [*Stern*, 2011; *Vannucchi et al*., 2013]. It is noteworthy that most blueschists reported in the central Qiangtang have been widely accepted as a result of the subduction of seamounts (or oceanic islands) based on the geochemical and Sr-Nd isotopic characteristics [*Kapp et al*., 2000; *Zhai et al*., 2011b; *Zhang et al*., 2014b]. The ages of these blueschists have been constrained as Permian (282–275 Ma) and Late Triassic (227–215 Ma) based on ^{40}Ar-^{39}Ar and Lu-Hf isochronal dating [*Deng et al*., 2000; *Zhai et al*., 2011a; *Pullen et al*., 2008]. Hence, multiple subduction of seamounts (or oceanic islands) widely occurring in the Paleo-Tethys oceanic crust could result in the significant subduction erosion process.

The peak metamorphic stage (M_2) of the Grt-St-Ms schists, characterized by the mineral assemblage of staurolite + muscovite + biotite + plagioclase ± potassium feldspar ± quartz, recorded amphibolite facies P-T conditions of 0.3–0.5 GPa and 470–520°C (>25°C/km) (Figure 9a). As the peak metamorphic temperature significantly higher than the ^{40}Ar/^{39}Ar closure temperature of muscovite [~400°C, *Harrison et al*., 2009], the muscovite ^{40}Ar/^{39}Ar ages (263–259 Ma) should reflect the timing when the rocks had cooled from 470 to 520°C at peak metamorphic stage down to ~400°C during the late exhumation process. The Ar-Ar isochronal dating of muscovite provide a minimum age for amphibolite facies metamorphism (>263 Ma) which is older than the timing of the closure of the Paleo-Tethys Ocean and the continental collision (Late Triassic) [*Song et al*., 2015; *Zhai et al*., 2011a; *Pullen et al*., 2008]. Synthesizing the previous studies and our new results, the amphibolite facies metamorphism (>263 Ma) could occur at oceanic subduction stage and be a response to the underplating and/or diapir process following the early subduction erosion. The evidence is listed as follows: (1) the peak P-T conditions of the Grt-St-Ms schists are significantly higher than those of Ordovician to Jurassic sedimentary sequences from NQB which were unmetamorphosed or underwent only greenschist-facies metamorphism [*Li and Zheng*, 1993; *Li*, 1987; *Zhang et al*., 2009; *Peng et al*., 2014], but is consistent with those of rocks formed in middle-lower crust at depths of 20–30 km [*Zhang et al*., 2014a]; (2) the near-isothermal decompression paths of eclogites and blueschists (Figure 9a) indicate a rapid exhumation process along the cold subduction channel [*Zhai et al*., 2011a; *Tang and Zhang*, 2014]. In contrast, the distinct warming decompression P-T path (from M_1 to M_2) of Grt-St-Ms schists suggests the rocks had been obviously heated during their ascent which is consistent with the tectonic processes of diapir into warm middle-lower crust rather than exhumation along the cold subduction channel. Therefore, the distinct P-T path of Grt-St-Ms schists reveal that the eroded materials experienced an underplating and/or diapir process following the early subduction (M_1) and underwent a strong overprinting of amphibolite facies metamorphism (M_2) within the warm middle-lower crust. The similar underplating and/or diapir process in many other subduction zones have been recognized and accepted as a general geodynamic process during subduction erosion [e.g., *Bassett et al*., 2010; *Stern*, 2011; *Contreras-Reyes et al*., 2014].

The significant subduction erosion in response to the subduction of seamounts (or oceanic islands) [*Kapp et al*., 2000; *Deng et al*., 2000; *Zhai et al*., 2011b; *Zhang et al*., 2014b] would result in an influx of buoyant materials eroded into the subduction channel. A sharp increase of buoyant materials in the subduction channel could trigger a forced return flow of subducted materials to underplate beneath the toe of the overriding plate [e.g., *Cloos and Shreve*, 1988; *Gerya et al*., 2002]. These low-density materials escaped from the cold subduction channel and rise upward into the warm middle-lower crust of the overriding plate under the influence of increasing buoyancy (Figure 9c). The disaggregation of the basement rocks of the upper plate in response to the subduction of seamounts may enhance the subsequent underplating and/or diapir of buoyant materials. The mechanism of this process is similar to the diapir and plumes in the mantle wedge which transported buoyant mélange rocks from the subduction channel to the source region of arc magmas [*Castro et al*., 2010; *Hasenclever et al*., 2011; *Marschall and Schumacher*, 2012], but it occurred in the much shallower depth (middle-lower crust rather than mantle wedge). The relatively hot (with higher

geothermal gradient) middle-lower crust led to the amphibolite facies metamorphic overprint (M_2) after the early blueschist facies (M_1) in the subduction channel, which defined the distinct clockwise and warming decompression P-T-t paths (Figures 9a and 9c). In summary, the P-T-t paths of the Grt-St-Ms schists from the central Qiangtang Block reveal a complete tectonic process including subduction erosion and the following underplating process, which is consistent with the observations based on seismic data from the current subduction erosion type continental margins [e.g., *Bassett et al*., 2010; *Contreras-Reyes et al*., 2014].

Based on the new petrological evidence above, significant subduction erosion processes have been recognized during the northward subduction of the Paleo-Tethys Ocean. The new interpretation in this study is consistent with many geological observations in central Qiangtang, such as the generally large-scale loss of arc magmatic rocks record, the irregular and sawtoothed suture zones, and the Early Paleozoic metamorphic rocks (basement?) which are widely exposed along the southern margin of the Northern Qiangtang Block (upper plate) (Figure 1b) [*Zhang et al*., 2014a]. The identification of subduction erosion during the northward subduction of the Paleo-Tethys Ocean will provide a starting point for more comprehensive future studies on crustal recycling, reconstruction of tectonic framework, and arc magmatism related to the evolution of the Paleo-Tethys Ocean.

6. Tectonic Implications and Conclusions

Subduction erosion has been gradually recognized from many modern convergent margins (e.g., NE Japan, Western USA, Peru, Costa Rica, Java, and Northern Chile) by investigations of marine geology, geophysics, boron, and lead isotope geochemistry, and numerical experiments [e.g., *von Huene and Scholl*, 1991; *von Huene et al*., 2004; *Goss and Kay*, 2006; *Vannucchi et al*., 2013; *Tonarini et al*., 2011]. Previous researches suggested that the majority of abraded materials would be subducted into the deep mantle to maintain the supercontinent cycle [*Scholl and von Huene*, 2009] while the rest could be incorporated into arc magmas [*Clift et al*., 2009; *Stern*, 2011; *Holm et al*., 2014] or returned and preserved in the orogens through subduction channels [*Zhang et al*., 2012; *Liu et al*., 2014]. Although the key process has been identified for years [e.g., *von Huene and Scholl*, 1991; *von Huene et al*., 2004], the general tectonic evolution process of subduction erosion is still enigmatic owing to a lack of crucial metamorphic records. In this contribution, we identify a set of peculiar medium-temperature metamorphic rocks (garnet-staurolite-muscovite schists) from a large number of LT/LP and LT/HP metamorphic rocks in the QMBT. These rocks were deposited in an active continental margin setting and metamorphosed in ongoing oceanic subduction stage before the Triassic collision. Most importantly, their P-T-t paths revealed a complete evolutional history for the general subduction erosion, including abrasion into the subduction channel, high-pressure metamorphism, and later underplating process. Moreover, the presence of medium-temperature metasedimentary rocks with a distinct clockwise and warming decompression P-T-t path could be an important indicator for determining a subduction erosion process in the other fossil subduction zones.

Acknowledgments
We sincerely thank the Editor Professor Cin-Ty Lee and an anonymous reviewer for their constructive suggestions, which greatly improved our manuscript. We also thank Lin-Li Cheng, Zheng-Yu Chen, Li Su, and Wen Chen for their assistance in the laboratory operations of EPMA, LA-ICP-MS dating, and $^{40}Ar/^{39}Ar$ dating. This study was jointly supported by the DREAM project of MOST China (2016YFC0600407), the Strategic Priority Research Program (B) of the Chinese Academy of Sciences (grant XDB03010600), the National Natural Science Foundation of China (41502054, 41372066, 41630208, 41573027, and 41421062), the Key Program of the Chinese Academy of Sciences (QYZDJ-SSW-DQC026), talent project of Guangdong Province (2014TX01Z079), the Guangzhou Institute of Geochemistry, Chinese Academy of Sciences (GIGCAS 135 Project (135TP201601), the Institute of Geology and Geological Survey Project of China (grant 1212011121243), and the China Postdoctoral Science Foundation funded project (grant 2015M572374). This is contribution IS-2332 from GIGCAS. The representative analyses of minerals data, zircon U-Pb data, $^{40}Ar/^{39}Ar$ stepwise heating dating data, and results of P-T evaluation are listed in the supporting information Tables S1–S4. They can be also obtained from Zhang (zhangxz@gig.ac.cn).

References

Bassett, D., R. Sutherland, S. Henrys, T. Stern, M. Scherwath, A. Benson, S. Toulmin, and M. Henderson (2010), Three-dimensional velocity structure of the Northern Hikurangi margin, Raukumara, New Zealand: Implications for the growth of continental crust by subduction erosion and tectonic underplating, *Geochem. Geophys. Geosyst. 11*, Q10013, doi:10.1029/2010GC003137.

Castro, A., T. V. Gerya, A. García-Casco, C. Fernández, J. Díaz Alvarado, I. Moreno-Ventas, and I. Loew (2010), Melting relations of MORB-sediment melanges in underplated mantle wedge plumes: Implications for the origin of Cordilleran-type batholiths, *J. Petrol., 51*, 1267–1295.

Cawood, P. A., C. J. Hawkesworth, and B. Dhuime (2012), Detrital zircon record and tectonic setting, *Geology*, *40*(10), 875–878.

Clift, P. D., P. Vannucchi, and J. P. Morgan (2009), Crustal redistribution, crust-mantle recycling and Phanerozoic evolution of the continental crust, *Earth Sci. Rev.*, *97*, 80–104.

Cloos, M., and R. L. Shreve (1988), Subduction-channel model of prism accretion, melange formation, sediment subduction, and subduction erosion at convergent plate margins. 1: Background and description, *Pure Appl. Geophys.*, *128*(3–4), 455–500.

Contreras-Reyes, E., J. Becerra, H. Kopp, C. Reichert, and J. Díaz-Naveas (2014), Seismic structure of the north-central Chilean convergent margin: Subduction erosion of a paleomagmatic arc, *Geophys. Res. Lett.*, *41*, 1523–1529, doi:10.1002/2013GL058729.

Deng, X. G., L. Ding, X. H. Liu, Y. An, P. A. Kapp, M. A. Murphy, and C. E. Manning (2000), Discovery of blueschists in Gangmar-Taoxing Co area, central Qiangtang [in Chinese with English abstract], Northern Tibet, *Acta Geol. Sin.*, *35*(2), 227–232.

Ernst, W. G. (1988), Tectonic history of subduction zones inferred from retrograde blueschist p-t paths, *Geology*, *16*(12), 1081–1084.

Fan, J. J., C. Li, M. Wang, C. M. Xie, and W. Xu (2015), Features, provenance, and tectonic significance of Carboniferous-Permian glacial marine diamictites in the Southern Qiangtang-Baoshan block, Tibetan Plateau, *Gondwana Res.*, *28*(4), 1530–1542, doi:10.1016/j.gr.2014.10.015.

Gehrels, G., et al. (2011), Detrital zircon geochronology of pre-Tertiary strata in the Tibetan-Himalayan orogen, *Tectonics*, *30*, TC5016, doi: 10.1029/2011TC002868.
Gerya, T. V., B. Stöckhert, and A. L. Perchuk (2002), Exhumation of high-pressure metamorphic rocks in a subduction channel: A numerical simulation, *Tectonics*, *21*(6), 1–19.
Goss, A. R., and S. M. Kay (2006), Steep REE patterns and enriched Pb isotopes in Southern Central American arc magmas: Evidence for forearc subduction erosion?, *Geochem. Geophys. Geosyst.*, *7*, Q05016, doi:10.1029/2005GC001163.
Harrison, T. M., J. Célérier, A. B. Aikman, J. Hermann, and M. T. Heizler (2009), Diffusion of 40 Ar in muscovite, *Geochim. Cosmochim. Acta*, *73*(4), 1039–1051.
Hasenclever, J., J. P. Morgan, M. Hort, and L. H. Rüpke (2011), 2d and 3d numerical models on compositionally buoyant diapirs in the mantle wedge, *Earth Planet. Sci. Lett.*, *311*(1), 53–68.
Hiroi, Y., Y. Ogo, and K. Namba (1994), Evidence for prograde metamorphic evolution of Sri Lankan pelitic granulites, and implications for the development of continental crust, *Precambrian Res.*, *66*(1–4), 245–263.
Holm, P. M., N. Søager, C. T. Dyhr, and M. R. Nielsen (2014), Enrichments of the mantle sources beneath the Southern Volcanic Zone (Andes) by fluids and melts derived from abraded upper continental crust, *Contrib. Mineral. Petrol.*, *167*(5), 1–27.
Hoskin, P. W. O., and L. P. Black (2000), Metamorphic zircon formation by solid-state recrystallization of protolith igneous zircon, *Journal of Metamorph. Geol.*, *18*, 423–439.
Jiang, Q. Y., C. Li, L. Su, P. Y. Hu, C. M. Xie, and H. Wu (2015), Carboniferous arc magmatism in the Qiangtang area, Northern Tibet: Zircon U-Pb ages, geochemical and Lu-Hf isotopic characteristics, and tectonic implications, *J. Asian Earth Sci.*, *100*, 132–144.
Kapp, P., A. Yin, C. E. Manning, M. Murphy, T. M. Harrison, M. Spurlin, D. Lin, X. G. Deng, and C. M. Wu (2000), Blueschist-bearing metamorphic core complexes in the Qiangtang block reveal deep crustal structure of northern Tibet, *Geology*, *28*(1), 19–22.
Kapp, P., A. Yin, C. E. Manning, T. M. Harrison, M. H. Taylor, and L. Ding (2003), Tectonic evolution of the early Mesozoic blueschist-bearing Qiangtang metamorphic belt, central Tibet, *Tectonics*, *22*(4), 1043, doi:10.1029/2002TC001386.
Krogh, E. J., and A. Råheim (1978), Temperature and pressure dependence of Fe-Mg partitioning between garnet and phengite, with particular reference to eclogites, *Contrib. Mineral. Petrol.*, *66*(1), 75–80.
Kukowski, N., and O. Oncken (2006), Subduction erosion—The "normal" mode of fore-arc material transfer along the Chilean Margin, in *The Andes: Active Subduction Orogeny*, edited by O. Oncken et al., chap. 10, pp. 217–236, Springer, Berlin.
Li, C. (1987), The Longmu Co-Shuanghu-Lanchangjiang plate suture and the north boundary of distribution of Gondwana affinity Permian-Carboniferous system in northern Tibet, China [in Chinese with English abstract], *J. Changchun Univ. Earth Sci.*, *17*(2), 155–166.
Li, C., and A. Zheng (1993), Paleozoic stratigraphy in the Qiangtang region of Tibet: Relations of the Gondwana and Yangtze continents and ocean closure near the end of the Carboniferous, *Int. Geol. Rev.*, *35*(9), 797–804.
Li, C., Q. G. Zhai, Y. S. Dong, and X. P. Huang (2006), Discovery of eclogite and its geological significance in Qiangtang area, central Tibet, *Chin. Sci. Bull.*, *51*(9), 1095–1100.
Liu, X., W. Su, J. Gao, J. Li, T. Jiang, X. Zhang, and X. Ge (2014), Paleozoic subduction erosion involving accretionary wedge sediments in the South Tianshan Orogen: Evidence from geochronological and geochemical studies on eclogites and their host metasediments, *Lithos*, *210*, 89–110.
Marschall, H. R., and J. C. Schumacher (2012), Arc magmas sourced from melange diapirs in subduction zones, *Nat. Geosci.*, *5*(12), 862–867.
Metcalfe, I. (2013), Gondwana dispersion and Asian accretion: Tectonic and palaeogeographic evolution of eastern Tethys, *J. Asian Earth Sci.*, *66*, 1–33.
Massonne, H. J., and W. Schreyer (1987), Phengite geobarometry based on the limiting assemblage with K-feldspar, phlogopite, and quartz, *Contrib. Mineral. Petrol.*, *96*(2), 212–224.
Peng, H., C. Li, C. M. Xie, M. Wang, Q. Y. Jiang, and J. W. Chen (2014), Riwanchaka Group in central Qiangtang Basin, the Tibetan Plateau: Evidence from detrital zircons [in Chinese with English abstract], *Geol. Bull. China*, *33*(11), 1715–1727.
Pullen, A., P. Kapp, G. E. Gehrels, J. D. Vervoort, and L. Ding (2008), Triassic continental subduction in central Tibet and Mediterranean-style closure of the Paleo-Tethys Ocean, *Geology*, *36*(5), 351–354.
Ranero, C. R., and R. Von Huene (2000), Subduction erosion along the middle America convergent margin, *Nature*, *404*, 748–52.
Scholl, D. W., and R. von Huene (2009), Implications of estimated magmatic additions and recycling losses at the subduction zones of accretionary (non-collisional) and collisional (suturing) orogens, in *Accretionary Orogens in Space and Time*, vol. 318, edited by P. Cawood and A. Kröner, pp. 105–125, Geol. Soc. of London, Spec. Publ., London.
Song, P., L. Ding, Z. Li, P. C. Lippert, T. Yang, X. Zhao, J. J. Fu, and Y. Yue (2015), Late Triassic paleolatitude of the Qiangtang block: Implications for the closure of the Paleo-Tethys Ocean, *Earth Planet. Sci. Lett.*, *424*, 69–83.
Stern, C. R. (2011), Subduction erosion: Rates, mechanisms, and its role in arc magmatism and the evolution of the continental crust and mantle, *Gondwana Res.*, *20*, 284–308.
Stern, R. J. (2005), Evidence from ophiolites, blueschists, and ultrahigh-pressure metamorphic terranes that the modern episode of subduction tectonics began in neoproterozoic time, *Geology*, *33*(7), 557–560.
Tang, X. C., and K. J. Zhang (2014), Lawsonite-and glaucophane-bearing blueschists from NW Qiangtang, northern Tibet, China: Mineralogy, geochemistry, geochronology, and tectonic implications, *Int. Geol. Rev.*, *56*(2), 150–166.
Tonarini, S., W. P. Leeman, and P. T. Leat (2011), Subduction erosion of forearc mantle wedge implicated in the genesis of the South Sandwich Island (SSI) arc: Evidence from boron isotope systematics, *Earth Planet. Sci. Lett.*, *301*(1), 275–284.
Vannucchi, P., P. B. Sak, J. P. Morgan, K. I. Ohkushi, and K. Ujiie (2013), Rapid pulses of uplift, subsidence, and subduction erosion offshore Central America: Implications for building the rock record of convergent margins, *Geology*, *41*(9), 995–998.
Velde, B. (1967), Si^{+4} content of natural phengites, *Contrib. Mineral. Petrol.*, *14*(3), 250–258.
von Huene, R., and D. W. Scholl (1991), Observations at convergent margins concerning sediment subduction, subduction erosion, and the growth of continental crust, *Rev. Geophys.*, *29*(3), 279–316.
von Huene, R., C. Ranero, and P. Vannucchi (2004), Generic model of subduction erosion, *Geology*, *32*, 913–916.
Wang, K., Y. Hu, R. Von Huene, and N. Kukowski (2010), Interplate earthquakes as a driver of shallow subduction erosion, *Geology*, *38*(5), 431–434.
Wu, C. M., and H. X. Chen (2015), Calibration of a Ti-in-muscovite geothermometer for ilmenite-and Al_2SiO_5-bearing metapelites, *Lithos*, *212*, 122–127.
Wu, C. M., and G. Zhao (2006), Recalibration of the garnet-muscovite (GM) geothermometer and the garnet-muscovite-plagioclase-quartz (GMPQ) geobarometer for metapelitic assemblages, *J. Petrol.*, *47*(12), 2357–2368.
Yang, T. N., H. R. Zhang, Y. X. Liu, Z. L. Wang, Y. C. Song, Z. S. Yang, S. H. Tian, H. Q. Xie, and K. J. Hou (2011), Permo-Triassic arc magmatism in central Tibet: Evidence from zircon U-Pb geochronology, Hf isotopes, rare earth elements, and bulk geochemistry, *Chem. Geol.*, *284*, 270–282.

Yin, A., and T. M. Harrison (2000), Geologic evolution of the Himalayan-Tibetan orogen, *Annu. Rev. Earth Planet. Sci.*, *28*, 211–280.
Zhai, Q. G., R. Y. Zhang, B. M. Jahn, C. Li, S. G. Song, and J. Wang (2011a), Triassic eclogites from central Qiangtang, northern Tibet, China: Petrology, geochronology and metamorphic P-T path, *Lithos*, *125*(1–2), 173–189.
Zhai, Q. G., B. M. Jahn, R. Y. Zhang, J. Wang, and L. Su (2011b), Triassic subduction of the Paleo-Tethys in northern Tibet, China: Evidence from the geochemical and isotopic characteristics of eclogites and blueschists of the Qiangtang Block, *J. Asian Earth Sci.*, *42*(6), 1356–1370.
Zhai, Q. G., B. M. Jahn, J. Wang, L. Su, X. X. Mo, K. L. Wang, S. H. Tang, and H. Y. Lee (2013a), The Carboniferous ophiolite in the middle of the Qiangtang terrane, Northern Tibet: SHRIMP U-Pb dating, geochemical and Sr-Nd-Hf isotopic characteristics, *Lithos*, *168*, 186–199.
Zhai, Q. G., B. M. Jahn, L. Su, J. Wang, X. X. Mo, H. Y. Lee, K. L. Wang, and S. Tang (2013b), Triassic arc magmatism in the qiangtang area, northern Tibet: Zircon U-Pb ages, geochemical and Sr-Nd-Hf isotopic characteristics, and tectonic implications, *J. Asian Earth Sci.*, *63*, 162–178.
Zhai, Q. G., B. M. Jahn, J. Wang, P. Y. Hu, S. L. Chung, H. Y. Lee, S. H. Tang, and Y. Tang (2016), Oldest paleo-tethyan ophiolitic mélange in the Tibetan plateau, *Geol. Soc. Am. Bull.*, *128*(3–4), 355–373.
Zhang, K. J., J. X. Cai, Y. X. Zhang, and T. P. Zhao (2006a), Eclogites from central Qiangtang, northern Tibet (China) and tectonic implications, *Earth Planet. Sci. Lett.*, *245*(3), 722–729.
Zhang, K. J., Y. X. Zhang, B. Li, Y. T. Zhu, and R. Z. Wei (2006b), The blueschist-bearing Qiangtang metamorphic belt (northern Tibet, China) as an in situ suture zone: Evidence from geochemical comparison with the Jinsa suture, *Geology*, *34*, 493–496
Zhang, J. X., J. P. Li, S. Y. Yu, F. C. Meng, C. G. Mattinson, H. J. Yang, and C. M. Ker (2012), Provenance of eclogitic metasediments in the north Qilian HP/LT metamorphic terrane, western China: Geodynamic implications for early Paleozoic subduction-erosion, *Tectonophysics*, *570*, 78–101.
Zhang, X. Z., Y. S. Dong, C. Li, M. R. Deng, L. Zhang, and W. Xu (2014a), Silurian high-pressure granulites from Central Qiangtang, Tibet: Constraints on early Paleozoic collision along the northeastern margin of Gondwana, *Earth Planet. Sci. Lett.*, *405*, 39–51.
Zhang, X. Z., Y. S. Dong, C. Li, C. M. Xie, M. Wang, M. R. Deng, and L. Zhang (2014b), A record of complex histories from oceanic lithosphere subduction to continental subduction and collision: Constraints on geochemistry of eclogite and blueschist in Central Qiangtang, Tibetan Plateau [in Chinese with English abstract], *Acta Petrol. Sin.*, *30*(10), 2821–2834.
Zhang, X. Z., Y. S. Dong, C. Li, M. R. Deng, L. Zhang, and W. Xu (2014c), Tectonic setting and petrogenesis mechanism of late Triassic magmatism in Central Qiangtang, Tibetan Plateau: Take the Xiangtao Lake pluton in the Hongjishan region as an example [in Chinese with English abstract], *Acta Petrol. Sin.*, *30*(2), 547–564.
Zhang, X. Z., Y. S. Dong, Q. Wang, W. Dan, C. Zhang, M. R. Deng, W. Xu, X. P. Xia, J. P. Zeng, and H. Liang (2016), Carboniferous and Permian evolutionary records for the Paleo-Tethys Ocean constrained by newly discovered Xiangtaohu ophiolites from central Qiangtang, central Tibet, *Tectonics*, *35*, 1670–1686, doi:10.1002/2016TC004170.
Zhang, Y. C., T. X. Yuan, Q. G. Zhai (2009), A preliminary report of the fieldtrip on the Carboniferous-Permian sequences in the north and south of the Longmu Co-Shuanghu suture zone, Northern Tibet in May and June, *Permophiles*, *53*, 5–7.
Zhu, D. C., Z. D. Zhao, Y. Niu, Y. Dilek, Z. Q. Hou, and X. X. Mo (2013), The origin and pre-Cenozoic evolution of the Tibetan Plateau, *Gondwana Res.*, *23*(4), 1429–1454.